Isotope shifts in francium isotopes $^{206-213}$Fr and ^{221}Fr

R. Collister and G. Gwinner
Department of Physics and Astronomy, University of Manitoba, Winnipeg, Canada MB R3T 2N2

M. Tandecki, J. A. Behr, and M. R. Pearson
TRIUMF, Vancouver, Canada BC V6T 2A3

J. Zhang and L. A. Orozco
JQI, Department of Physics and NIST, University of Maryland, College Park, Maryland 20742, USA

S. Aubin
Department of Physics, College of William and Mary, Williamsburg, Virginia 23186, USA

E. Gomez
Instituto de Física, Universidad Autónoma de San Luis Potosí, San Luis Potosi 78290, Mexico
(FrPNC Collaboration)

(Received 4 June 2014; published 7 November 2014)

We present the isotope shifts of the $7s_{1/2}$ to $7p_{1/2}$ transition for francium isotopes $^{206-213}$Fr with reference to ^{221}Fr collected from two experimental periods. The shifts are measured on a sample of atoms prepared within a magneto-optical trap by a fast sweep of radio-frequency sidebands applied to a carrier laser. King plot analysis, which includes literature values for $7s_{1/2}$ to $7p_{3/2}$ isotope shifts, provides a field shift constant ratio of 1.0520(10) and a difference between the specific mass shift constants of 170(100) GHz amu between the D_1 and D_2 transitions, of sufficient precision to differentiate between *ab initio* calculations.

DOI: 10.1103/PhysRevA.90.052502 PACS number(s): 32.10.Fn, 31.30.Gs, 37.10.Jk, 42.62.Fi

I. INTRODUCTION

The variation in the atomic transition energy between isotopes of the same element is known as the isotope shift. It arises due to a combination of nuclear and atomic effects, requiring detailed knowledge of both for accurate predictions. Isotope shifts provide information about the nuclear charge distribution (for examples, see [1,2]) and are sensitive to electron correlations. They have been employed in the search for space and time variation of the fine-structure constant (α) [3] and play a role where accurate spectroscopic information is required, for example when calculating stellar element abundances [4].

Francium, with its high nuclear charge ($Z = 87$) and relatively simple, alkali electronic configuration, has attracted a lot of attention as a candidate for fundamental symmetry tests [5–7]. These investigations require a thorough knowledge of both the atomic and nuclear structure, in particular the overlap of the electronic wave functions with the nucleus, to which optical isotope shifts are sensitive. The interpretation of atomic parity nonconservation measurements also relies on accurate many-body theory [8], for which isotope shifts provide benchmarks.

In the present work, we measure the optical isotope shift between laser-trapped, cold francium isotopes (see Fig. 1). The isotope shift can be separated into two distinct parts: the field shift, caused by variation in the charge distribution in the nucleus, and the mass shift, caused by the different kinetic energy of the finite-mass nucleus. For a complete treatment of the optical isotope shift, see Refs. [9,10].

The mass shift comes directly from the changing mass of the nucleus. In the center-of-mass frame,

$$\Delta E = \mathbf{P}^2/2M = \left(\sum_i \mathbf{p}_i\right)^2 \Big/ 2M, \tag{1}$$

where M is the nuclear mass, $\mathbf{P}$ is the nuclear momentum, and $\mathbf{p}_i$ is the momentum of the ith electron. In all but the lightest of elements, the mass shift can be separated into two parts:

$$\Delta E = \frac{1}{2M}\sum_i {\mathbf{p}_i}^2 + \frac{1}{M}\sum_{i>j} \mathbf{p}_i \cdot \mathbf{p}_j, \tag{2}$$

where the first term, i.e., the normal mass shift or Bohr reduced mass effect, can be determined exactly and the second term, i.e., the specific mass shift arising from the change in momentum correlations between electrons, is much more difficult to calculate.

Isotope shifts are measured with respect to a reference isotope. The contribution of the normal mass shift to the frequency shift of an optical transition is

$$\delta\nu_{NMS}^{AA'} = \nu(A')\frac{m_e(M_A - M_{A'})}{M_{A'}(M_A + m_e)}, \tag{3}$$

where $\nu(A')$ is the transition frequency of the reference isotope with mass number A', $M_A(M_{A'})$ is the nuclear mass of the measured (reference) isotope, and m_e is the mass of the electron, which can be neglected in the denominator. The electron correlations for the specific mass shift must be very well known in order to check the theoretical models used to extract, e.g., the time variation of α [3]. Francium, as the heaviest alkali, is more tractable than multivalence electron systems such as lead, making it very suitable for testing calculations. Together, the total mass shift $\delta\nu_{MS}$ between isotopes of mass numbers A and A', and following the form of Eq. (3), can be written as

$$\delta\nu_{MS}^{AA'} = (N + S)\frac{M_A - M_{A'}}{M_A M_{A'}}, \tag{4}$$

where N, S are the normal and specific mass shift constants.

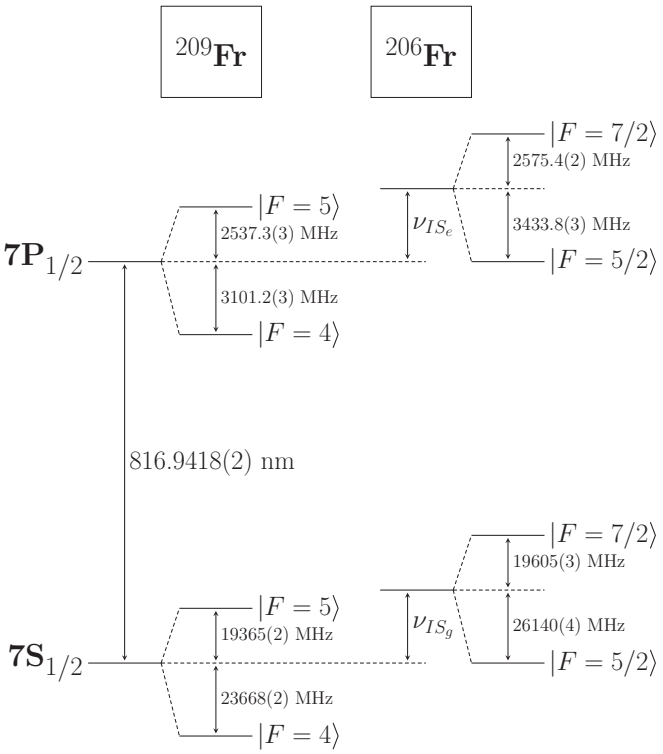

FIG. 1. Energy-level diagram of ^{209}Fr and ^{206}Fr showing the $7s_{1/2}$ and $7p_{1/2}$ levels. The isotope shift of the D_1 line is measured between the centers of gravity of the ground and excited states comprising the transition, i.e., the difference between the isotope shifts of those two states ($\nu_{IS_e} - \nu_{IS_g}$).

The field shift is due to the modification of the point-charge Coulomb potential by a finite-size nucleus. This results in a contraction of the spacings between electronic bound-state energies of an atom. The contraction is isotope dependent so that there is a difference in the transition frequency between isotopes,

$$\delta\nu_{FS}^{AA'} = F\delta\langle r^2\rangle^{AA'}, \tag{5}$$

where $\delta\langle r^2\rangle^{AA'}$ is the difference in the mean nuclear charge radii squared of the two isotopes. The field shift constant F is

$$F = -\frac{\pi a_0^3}{Z}\Delta|\psi(0)|^2 f(Z), \tag{6}$$

where $\Delta|\psi(0)|^2$ is the change of the electron charge density at the nucleus between the states involved in the transition and $f(Z)$ is an increasing function of Z that accounts for relativistic and nuclear shape corrections.

The sum of mass and field shifts gives the total isotope shift,

$$\delta\nu_{IS}^{AA'} = (N+S)\frac{M_A - M_{A'}}{M_A M_{A'}} + F\delta\langle r^2\rangle^{AA'}, \tag{7}$$

which we measure in our experiment and compare to theoretical predictions.

II. EXPERIMENTAL SETUP

We trap neutral francium atoms in a magneto-optical trap (MOT) at the Francium Trapping Facility at TRIUMF in Vancouver, Canada [11]. Francium has no stable isotopes; the TRIUMF Isotope Separator and Accelerator (ISAC) facility delivers up to 10^9 Fr ions s^{-1}, which are high rates for radioactive beam standards, and we trap them to achieve the large densities conducive to high-precision measurements. A 500 MeV, 10 μA proton beam impinges upon a uranium carbide (UCx) target to produce a large range of isotopes. The products are surface ionized on a hot ($\sim$2200 °C) rhenium-coated tantalum tube, accelerated to $\sim$20 keV, and then mass selected by passing through a pair of magnetic dipoles. The francium ions are delivered to the experiment where they accumulate in an yttrium neutralizer foil that is rotated and heated for 1 s, causing the now neutral atoms to emerge from the foil and enter the trapping volume on a 20 s cycle. Roughly 2.5×10^5 atoms with trap lifetime >10 s for ^{209}Fr are initially trapped before trap losses and radioactive decays reduce that number in the time between yttrium heating pulses. A schematic of the experimental apparatus is available in Fig. 4 of Ref. [11].

The isotope shift measurements we have performed involve the fast radio-frequency (rf) scan of sidebands on a carrier (probe) laser to locate specific transitions in a particular isotope with respect to a reference one. Figure 2 depicts the measurement scheme. First, we collect one isotope in the MOT, such as ^{206}Fr in Fig. 2, tune the probe laser frequency to lie in the hyperfine multiplet of the D_1 line originating from the upper hyperfine ground state, and sweep the sideband frequency in 10 ms to find the transition. Next, we change the isotope in the trap, to, e.g., ^{209}Fr, and sweep the rf sidebands again to find the desired transition while the carrier remains locked. The measured difference in rf frequencies is used to calculate the isotope shift. Data collection occurred during two experimental periods using two different rf generation schemes (details below). In the first period, we measured the isotope shifts of ^{206,207,213}Fr with respect to ^{209}Fr, while the second yielded $^{206,208-212,221}$Fr with a fixed laser position and no need to return to a reference for each new isotope.

Our rf sideband method finds the transitions to both excited hyperfine levels. Thus we also obtain the hyperfine splittings to 100 ppm precision, which is sufficient to study changes in the hyperfine anomaly [12]. The hyperfine splittings and nuclear spin are required to calculate the hyperfine shifts of the ground and excited states, which are different for each isotope. These are necessary to extract the isotope shift since we need to locate the center of gravity of the transition. We determine the isotope shift from

$$\delta\nu_{IS} = (\nu_1 - \nu_2) + (\nu_{HF_g} - \nu_{HF_e}) - (\nu_{HF_g} - \nu_{HF_e})_{ref}, \tag{8}$$

where $\nu_{1,2}$ are the rf frequencies where the hyperfine transitions are observed (see Fig. 2), and $\nu_{HF_{g(e)}}$ are the hyperfine shifts of the ground (excited) states for the measured isotope and the reference. The common probe laser frequency is not included, as it cancels out. The hyperfine shifts are given by

$$\nu_{HF} = \frac{\nu_{HFS}}{2I+1}[F(F+1) - I(I+1) - J(J+1)], \tag{9}$$

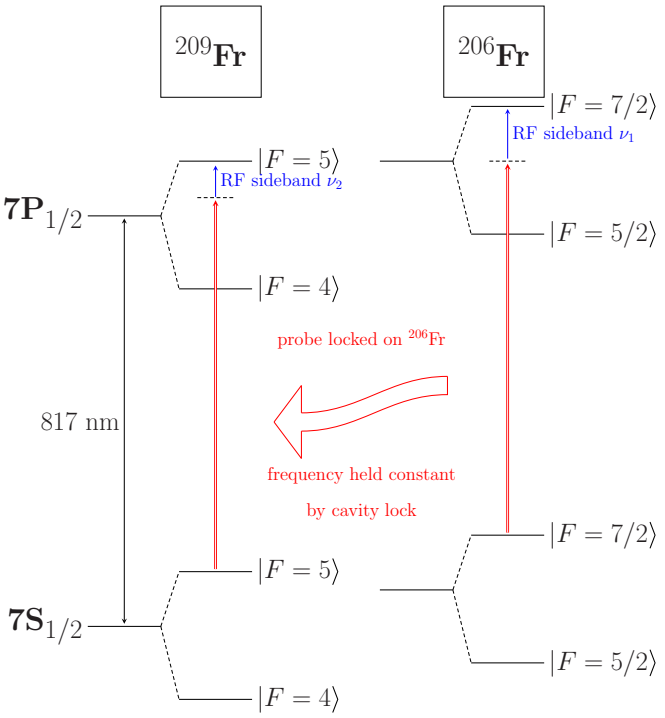

FIG. 2. (Color online) Isotope shift measurement scheme; splittings not to scale. The transition to the upper hyperfine excited state $F = 7/2$ is located in ^{206}Fr and the probe laser frequency is locked using the external Fabry-Perot cavity. Then ^{209}Fr is trapped and the transition to $F = 5$ is located by changing the rf frequency only, leaving the carrier laser frequency unchanged. This difference in rf frequencies gives the D_1 transition isotope shift once we know the hyperfine shifts (see Fig. 1).

where ν_{HFS} is the hyperfine splitting, and I, J, and F are the nuclear spin, electronic, and total angular momentum quantum numbers, respectively.

Our method of setting the carrier laser frequency between the hyperfine levels allows a clean extraction of the total $7p_{1/2}$ splitting independent of the exact carrier laser frequency. The difference of the observed transition centroids in a single scan is the hyperfine splitting; any shift in one centroid position caused by laser offset is canceled by a corresponding shift in the other centroid, assuming there is no laser drift during a single rf sweep.

The probe laser frequency is locked to this position via a scanning Fabry-Perot cavity and a stabilized Melles-Griot 05-STP-901 HeNe laser, transferring the long-term stability of the HeNe to the other laser (for details, see [11,13]). We keep the probe laser locked during the isotope change in the MOT. The probe laser is a Ti:sapphire laser operating at 817 nm; we send linearly polarized light into an EOSpace AZ-2K1-10-PFA-PFA-800-UL amplitude modulator for sideband generation. A fiber carries the probe light to the atoms, and the light is retroreflected to minimize any pushing of the atoms as they scatter photons. The 10 mW/cm^2 in each sideband is enough to saturate the transition, and the fluorescence collects in our detection system (details below) when a sideband frequency is resonant with a hyperfine level.

The laser light for the MOT [14] is produced by a pair of commercial Ti:sapphire ring lasers operating at 718 nm. They are coupled into a fiber splitter to generate the three spatial beams at two frequencies that are retroreflected to trap on each axis. Laser powers delivered to the trap are limited by the coupling fibers, resulting in approximately 20 mW/cm^2 in the trapping beams and 5 mW/cm^2 in the repumping beams; all beams have $1/e^2$ power diameters of 5 cm. Quadrupole magnetic field coils provide a field gradient of 7 G/cm (strong axis). The typical detuning of the trap laser is about 15 MHz, roughly two and a half linewidths detuned to the red. Once the transitions are found, the lasers are locked to the stabilized HeNe via the scanning Fabry-Perot cavity. The stability of the laser-lock system is important and will be discussed below.

Sidebands are generated by an rf signal applied to the fiber modulator, consisting of a lithium niobate electro-optic modulator in one arm of a Mach-Zehnder interferometer. A YYLabs Mini-MBC-1 modulation bias controller card gives a bias voltage to the modulator to keep the carrier suppressed. This increases the power to the sidebands and reduces the scattered light from the carrier.

Two different rf synthesizer setups have been used to measure the isotope shifts. One, employed during the first experimental data collection period, involves Analog Devices (AD) AD4350 synthesizers mounted on a pair of UG-110 evaluation boards to generate the rf frequencies desired. The boards operate using a phase-locked loop (PLL) stabilized voltage controlled oscillator (VCO) referenced to a 10 MHz clock. A continuous output frequency sweep is performed by manipulating the input clock frequency using a Stanford Research Systems DS345 function generator. The scanning range (70 MHz) of one frequency synthesizer is limited to how far the clock can be moved off the nominal set point before the PLL is lost and the VCO becomes unlocked, resulting in output instability and unresponsiveness to further clock manipulation. This frequency-dependent range, along with the 4.4 GHz maximum frequency, limits the isotopes we could measure with these boards using ^{209}Fr as a reference. Two of the boards are employed along with an rf switch synchronized with the clock sweep to pass the correct synthesizer output allowing for ~140 MHz of continuous frequency scanning.

The second rf setup, used for the second data collection period, uses a Phase Matrix QuickSyn FSW-0020, a direct digital synthesizer using a fundamental VCO and PLL to generate frequencies from 0.5–20 GHz. This synthesizer allows us to tune the probe laser sidebands to any of the D_1 transitions in the isotopes we trap. The output sweep is digitally controlled stepwise at a maximum 7 kHz rate, giving us 70 frequency steps in the 10 ms allocated for each measurement. The probe lockpoint is maintained for all isotopes and the sideband frequency is tuned to locate both D_1 transitions for each isotope once it is trapped. Thus this setup has the additional advantage of not requiring a return to a reference isotope for each subsequent measurement.

On-resonance scattered light is collected by a double-relay optical system and detected by a Hamamatsu H7422 photomultiplier tube (PMT). An interference filter centered at 820 nm and an edge filter with 795 nm cut-on wavelength are in place to block light other than the D_1 line scattered photons in order to reduce background counts. A Stanford Research

Systems SR430 multichannel scaler (MCS) collects the signal from the PMT as a function of time. The MOT operates with trap and repumper lasers on the D_2 line at 718 nm and thus they do not contribute appreciably to the background.

In order to minimize ac Stark shifts of the $7s$ ground state, the trap laser light is extinguished periodically during the 10 ms rf sweep on a 32 μs cycle of 50 MCS bins that are each 640 ns long. The chopping cycle is 21.76 μs (34 bins) with the light on, followed by 7.04 μs (11 bins) with the light extinguished by an acousto-optic modulator with a greater-than-10^4 extinction factor, and ended by the remaining 3.2 μs (5 bins) with the light back on.

III. RESULTS

We measure the D_1 isotope shifts for isotopes $^{206-213}$Fr with respect to ^{221}Fr. Analysis of the data yields the frequency difference between isotopes of the hyperfine transitions, which we use to calculate the isotope shift [see Fig. 1 and Eq. (8)]. The splittings of the $p_{1/2}$ level are obtained by taking the difference of the sideband frequencies of the two transitions from a single scan [see Fig. 3(a)]. Our reported isotope shifts are ultimately calculated with reference to ^{221}Fr and we recalculate the literature D_2 isotope shifts from reference ^{212}Fr to ^{221}Fr for the King plot analysis which follows.

To obtain the transition frequency difference, we calibrate the frequency of each MCS bin by measuring the output of our frequency generators. The outputs of the latter are mixed down to allow the wave forms to be observed directly on an oscilloscope, where they are captured to be fit to sinusoids at fixed times during the 10 ms scan. The fitted frequencies show that both the AD cards and Phase Matrix synthesizer behave as expected as long as the AD cards remain phase locked to their input clocks. All measured frequencies are as predicted with uncertainties of less than 10 kHz, enabling us to construct a linear frequency-time correspondence of the rf, which we use to calibrate the MCS.

The peaks in the data are fit with Lorentzians on a quadratic background using the ROOT analysis package to determine the centroid of each transition. We do not consider the effect of trap losses or nuclear decays on the fit, as the 10 ms scan length is much shorter than the 20 s lifetime of the trap or the 15 second to 20 minute half lives of the isotopes. Statistical uncertainties from these fits are less than 100 kHz and in some cases less than 15 kHz. The peaks typically have Lorentzian widths of 8 MHz for data collected with the trap light off; this is partly due to saturation broadening of the 5.4 MHz natural linewidth, calculated from the measured lifetime of the $7p_{1/2}$ state [15].

An example scan is provided in Fig. 3 for the ^{206}Fr to ^{209}Fr D_1 isotope shift. Table I summarizes the results; the reported errors for the D_1 isotope shifts are the quadratic sums of the measurement error, and hyperfine shift errors, calculated from $A(s_{1/2})$ and $A(p_{1/2})$ errors and nuclear spins, for both the measured isotopes and the reference ^{221}Fr. Additionally, we measured the $7p_{1/2}$ hyperfine splitting of ^{206}Fr^m ($t_{1/2} \approx 16$ s) to be 6524.3(6) MHz and the shifts with respect to ^{221}Fr for the

TABLE I. Overview of our measurements and literature values that are relevant for calculating isotope shifts to be used for a King plot. Literature D_2 isotope shifts ($\delta\nu_{IS}$) are reported with ^{212}Fr as the reference, with the exception of the ^{206}Fr D_2 value, which is measured with respect to ^{208}Fr. They have been recalculated using the ^{212}Fr to ^{221}Fr isotope shift from [16] to be common with our D_1 isotope shifts. Nuclear spins and $A(S_{1/2})$ values are from the literature and $A(P_{1/2})$ are from our measurements [12]. The final isotope shift uncertainty reported in parentheses is a combination of our measurement uncertainty and the A coefficient uncertainties needed to calculate the centers of gravity.

	This work		Literature values			
Isotope	$A(P_{1/2})$ (MHz)	$D_1\delta\nu_{IS}$ (MHz)	Spin	$A(S_{1/2})$ (MHz)	$D_2\delta\nu_{IS}$ (MHz)	Source
206	1716.9(2)	29175(5)	3	13052.2(20)	30684(5)	[17]
207	1111.9(1)	27432(6)	9/2	8484.(1)	28809(5)	[16]
208	874.68(8)	27210(4)	7	6650.7(8)	28573(4)	[16]
209	1127.7(1)	25432(3)	9/2	8606.7(9)	26698(4)	[16,18]
210	946.33(9)	24927(3)	6	7195.1(4)	26178(4)	[16,18]
211	1142.1(1)	23300(5)	9/2	8713.9(8)	24465(4)	[16,18]
212	1192.2(1)	22437(4)	5	9064.4(15)	23570(2)	[16,19]
213	1147.9(1)	20869(7)	9/2	8757.4(19)	21929(3)	[16,19]
221	811.5(2)	0	5/2	6209.9(10)	0	[16,19]

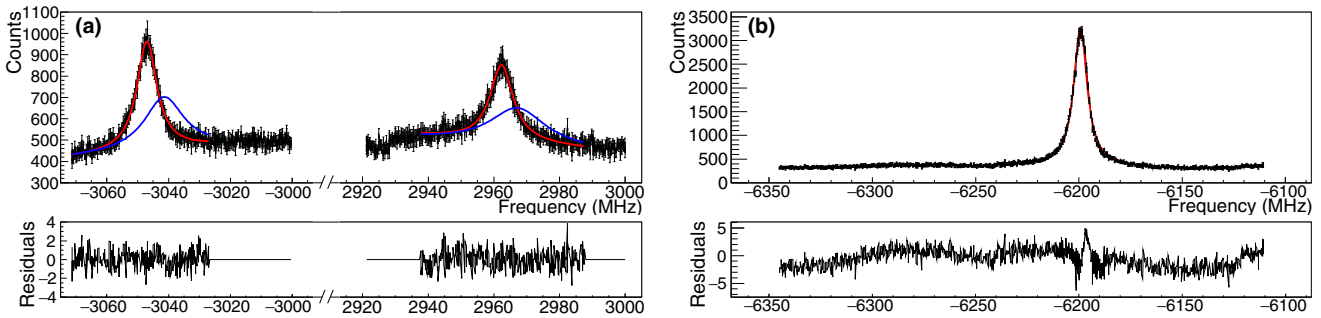

FIG. 3. (Color online) Data of (a) the $7p_{1/2}$ splitting of ^{206}Fr and (b) the reachable transition in ^{209}Fr using the AD4350 rf generator along with the normalized residuals of their fits. The Lorentzian fits on a quadratic background are shown (red line). The hyperfine splitting of the excited state is obtained from scans such as (a), where it is the difference of the centroids of both peaks. The blue lines show the ac Stark shifted peaks in the presence of the trapping laser light (data points not shown). The reference isotope measurement for the isotope shift shows a single transition peak; the other is roughly 6 GHz away, well outside the range of our scan. Transitions are identified by knowing the directions of both the probe laser detuning from the midpoint and rf sweep.

D_1 transition (i.e., rf frequencies $\nu_1 - \nu_2$) to be 11774(2) MHz for the transitions involving the lower $7p_{1/2}$ states and 15864(2) MHz for the upper $7p_{1/2}$ states. Without knowing the nuclear spin or the $A(s_{1/2})$, we cannot extract an isotope shift or $A(p_{1/2})$ value from those measurements.

The dominant systematic effect in our isotope shift measurement is given by the laser-lock drift; all other contributions are well below this one. Other sources of systematic error are ac Stark shifts, Zeeman shifts, and background contributions. These are more important for the hyperfine splitting measurement as laser drift in this case causes a broadening but no shift in the observed transition energy.

Our laser-locking system exhibits slow drifts over the time between measurements as the isotope in the trap was changed. This involves changes in the mass separator of the ISAC facility as well as changing the laser frequencies, and took between 30 to 60 minutes before the next isotope was measured. Long-term observations of the Fabry-Perot cavity and helium-neon laser exhibited drifts below 3 MHz over periods of one hour for the system in use during the first experiment. The drift was determined by feeding into the cavity a laser stabilized via saturated absorption spectroscopy in rubidium. We discovered the drift was largely due to uncontrolled feedback by back reflection from optical surfaces into the HeNe laser, temperature drift-induced expansion of the cavity tube, and nonlinearity of the piezo scanning the cavity length. Thus, for our first isotope shift measurements, we conservatively place the sum of systematic errors at ± 3 MHz, dominated by the laser-lock drift. Many of these laser stability issues were improved for the second set of measurements; we introduced an optical isolator to prevent feedback into the HeNe, the cavity is held under vacuum and is temperature locked via proportional-integral-derivative control, and we lock the probe laser to a frequency such that its locking peak in the cavity nearly coincides with that of the HeNe, suppressing piezo nonlinearity effects on the measurement. These improvements reduce the systematic error of the laser drifts to below ± 2 MHz.

The ac Stark shift of the ground state by the D_2 line excitation is eliminated by chopping the trapping laser light while the rf sideband sweep is occurring. For the splitting measurements, any shift present is canceled to first order by having the probe frequency set between the two transition frequencies; any change in the ground state shifts the measured transition frequencies the same amount, which cancels when taking the difference. The repumper frequency is set an isotope-dependent approximate 43 GHz away, making its contribution to the Stark shift negligible. The ac Stark shift of the ground state from the off-resonance probe laser sideband is estimated at less than 180 kHz based on measured intensity and detunings.

Zeeman shift is due to nonzero magnetic fields across the atom cloud in the trap and must be accounted for as the quadrupole magnetic field of the MOT remained on when taking a measurement. The effect of the magnetic field is estimated by two methods: varying the current in the quadrupole coils generating the field and changing the polarization of the light exciting the D_1 transition. The change in polarization will induce transitions between different magnetic sublevels or m_F states by the usual selection rules, each of which has a m_F-dependent Zeeman shift. Furthermore, even with perfectly linear light, we would still induce $\Delta m_F = 0, \pm 1$ due to the changing direction of the quadrupole field around the zero point. We performed these tests both online with francium and offline with rubidium; both alkalis have very similar behavior in magnetic fields. Altogether, the measurements place an upper bound on the contribution to the systematic error by the magnetic field of 540 kHz.

Background counts are minimized by the spatial filtering of the imaging system: a double relay with an aperture at the image plane. An interference filter centered around 820 nm in front of the PMT and chopping the trap laser during measurement also reduce background counts. Additionally, proper control of the fiber modulator voltage bias greatly suppresses the intensity of the carrier output, reducing its contribution to background. We did observe fluctuations in the shape of the background. These are likely caused by drifts in the phase between paths through the amplitude fiber modulator, due to small changes in temperature or bias voltage, resulting in more background light at the carrier frequency. Investigating this effect over many scans by fitting with different-order polynomials changes the fit centroid less than 100 kHz and we add this to the systematic uncertainty.

Additionally, there is a systematic uncertainty introduced from the literature $A(s_{1/2})$ values that we use to calculate the ground-state hyperfine shift [16–19] required to find the center of gravity and hence the isotope shift. Measurement of this quantity constitutes an entirely different experimental technique, and we do not currently have the means to measure these 40–50 GHz splittings ourselves. Therefore, we add the 1–4 MHz uncertainties calculated from the published ground-state values to our isotope shift measurement uncertainty.

IV. KING PLOT ANALYSIS

In all but the lightest nuclei, a King plot [10] separates the mass and field shift components of the isotope shift and allows comparison between different atomic transitions. The plot requires isotope shifts for two atomic transitions as well as the masses [20] of the isotopes measured. Our measurements on the D_1 line along with existing data for the D_2 line [16–18] provide shifts in eight francium isotopes with respect to ^{221}Fr. Taking Eq. (7) for two transitions and combining them to eliminate $\langle r^2 \rangle^{AA'}$ gives

$$\left(\frac{M_A M_{A'}}{M_A - M_{A'}}\right)\delta\nu_{IS,D2} = (N_{D2} + S_{D2}) - (N_{D1} + S_{D1})\frac{F_{D2}}{F_{D1}} + \frac{F_{D2}}{F_{D1}}\left(\frac{M_A M_{A'}}{M_A - M_{A'}}\right)\delta\nu_{IS,D1}, \tag{10}$$

a linear equation in isotope shifts weighted by isotopic masses, which we shall call the modified isotope shifts (MIS), with a slope given by the ratio of the field shift constants and intercept dependent on the differences in the mass shift constants. The normal mass shift can be calculated exactly; thus the intercept can be used to determine the difference in specific mass shift constants. A deviation from unity of the slope tells the ratio of the electronic overlap with the nucleus of the $7p_{1/2}$ and $7p_{3/2}$ states.

The King plot in Fig. 4 uses isotopes $^{207-213}$Fr, with ^{221}Fr as a reference; ^{206}Fr is excluded from the fit for reasons discussed below. We find that $F_{D2}/F_{D1} = 1.0520(10)$ and $(N_{D2} + S_{D2}) - (N_{D1} + S_{D1})\frac{F_{D2}}{F_{D1}} = 190(100)$ GHz amu with $\chi^2/ndf = 4.996/5$. The normal mass shift constants are $N_{D1} = 201$ and $N_{D2} = 229$ GHz amu from Eq. (3) with negligible errors given by the uncertainty in atomic masses. This leaves the specific mass shift constant difference ($\delta\mathcal{S}$) between the two transitions $\delta\mathcal{S} = S_{D2} - S_{D1}\frac{F_{D2}}{F_{D1}} = 170(100)$ GHz amu.

The outlier of ^{206}Fr (labeled in red in Fig. 4) requires a comment. This isotope was measured in our two data collections with results in agreement with each other from the different methods, suggesting it is not a measurement error. There is a 10σ deviation from the straight-line fit that we are unable to explain. Including this isotope in the fit produces a $\chi^2/ndf = 38.6/6$, again with the point falling 6σ away from the fit line; thus it is likely that there is some physical reason for the discrepancy. Evaluation of the complicated considerations in a more complete field shift theory [21] proves insufficient to explain this discrepancy; we are not at a sensitivity to observe those higher-order effects, which come in at the few MHz level and are within our error bars. It is possible some nuclear effect is responsible for this deviation; the unusual nuclear magnetic dipole and spectroscopic electric quadrupole likewise suggest the ^{206}Fr nucleus deviates from the behavior exhibited by the heavier $A \leqslant 213$ isotopes [17].

There is a known correction to the field shift from the electronic density changing over the nuclear volume, which depends on the nuclear charge distribution [21]. The corrections in $\delta\langle r^4\rangle$ and $\delta\langle r^6\rangle$ can be related in various basic nuclear charge distributions to the change in charge radii $d\langle r^2\rangle/dA$ [22]. This quantity then shows odd-even staggering. However, such a phenomenological correction would be within the errors of our measurements, and an inspection of the residuals in Fig. 4 show no significant difference between the odd-odd and even-even isotopes. This effect is unable to account for our discrepancy.

Furthermore, these higher-order corrections make the field shift coefficients F isotope dependent. Thus, since we are mainly concerned with the atomic calculations behind the isotope shift *N,S,F* values as predicted from theory, we will exclude ^{206}Fr from the linear fit used to evaluate those coefficients.

Using ^{212}Fr as the reference isotope minimally shifts the fit results. The χ^2/ndf is slightly poorer at 5.047/5 and the slope has moved 0.5σ to 1.0526(7). The change in the fit is due to the systematic errors in the measurement of the reference isotope; that common error is now with respect to ^{212}Fr instead of ^{221}Fr. Furthermore, using ^{212}Fr as the reference puts the ^{221}Fr King plot point in a location that dominates the fit. Therefore, we will continue to use ^{221}Fr as the reference isotope.

Calculations for the field shift and specific mass shift constants have been performed using several methods: many-body perturbation theory and closed-cluster approaches [8], as well as many-body perturbation theory calculation [23]. Our results and their predictions are summarized in Table II for the field shifts and Table III for the specific mass shifts. In Table III, the finite field result uses the average of three different methods which vary in their consideration of higher-order effects and the fourth column uses the $(SD + E3)$ value from Table II for F_{D2}/F_{D1} for the results from [8]. Using the $[BO(\Sigma^\infty)]$ value instead would cause no change at this sensitivity. The fit of the King plot agrees with the field shift constants predicted by the closed-cluster method $(SD + E3)$ at the 1σ level and with the perturbation theory $[BO(\Sigma^\infty)]$ method at the 2σ level, and does not agree with the prediction from [23]. The specific mass shift constants extracted from this King plot intercept agree with the finite field and Mårtensson-Pendrill (M-P) results at the 1σ level and the perturbation theory at the 2σ level.

TABLE II. Field shift constants (MHz/fm^2) obtained from three theoretical methods along with the experimental ratio (uncertainty) obtained from the King plot analysis shown in Fig. 4.

Method	$7S_{1/2}$	$7P_{1/2}$	$7P_{3/2}$	F_{D2}/F_{D1}
$BO(\Sigma^\infty)$[a]	−20463	−693	303	1.0504
$SD + E3$[a]	−20188	−640	361	1.0512
M-P[b]	−20782	−696	245	1.0468
Expt. (this work)				1.0520(10)

[a]Dzuba, Johnson and Safronova [8].
[b]Mårtensson-Pendrill (M-P) [23]

We can also fix the F_{D2}/F_{D1} ratio to theory and see what specific mass shift constants fit our data. The slope of the King plot is set in turn to the theory values and the resulting $\delta\mathcal{S}$ are displayed in Table III. These $\delta\mathcal{S}$ exhibit a linear trend as a function of field shift ratio. Fitting this line results in

$$\delta\mathcal{S} = (102 \pm 2) \times 10^3 \left(\frac{F_{D2}}{F_{D1}} - 1.0520\right) + 170 \pm 7, \quad (11)$$

allowing a $\delta\mathcal{S}$ value (in GHz amu) to be calculated from our measurements for any future field shift theory predictions.

The deviation from unity in the experimental King plot slope of 0.0520(10) corresponds to a 2% measurement. The total ratio has been measured to 0.1%, well below the stated 1% accuracy of the theory [8]. This analysis is limited by our reliance on previous D_2 line measurements and the ground-state hyperfine A coefficients extracted from those measurements. Our D_1 isotope shift uncertainties are inflated

TABLE III. Specific mass shift constants (GHz amu) obtained from three theoretical methods along with the experimental value (uncertainty) obtained from the King plot analysis shown in Fig. 4. The results from fixing the King plot slope to the different theory values are also shown.

Method	$7S_{1/2}$	$7P_{1/2}$	$7P_{3/2}$	$\delta\mathcal{S}$
PT[a]	−786.1	−53	7.9	24
FF[a]	−237	−62	77	130
M-P[b]	−570	−154	−18	117
Expt. (this work)				170(100)
Fixed slope $BO(\Sigma^\infty)$				90(9)
Fixed slope $SD + E3$				8(9)
Fixed slope M-P				−359(9)

[a]Perturbation theory (PT) and finite field (FF) approaches [8].
[b]Mårtensson-Pendrill (M-P) [23]

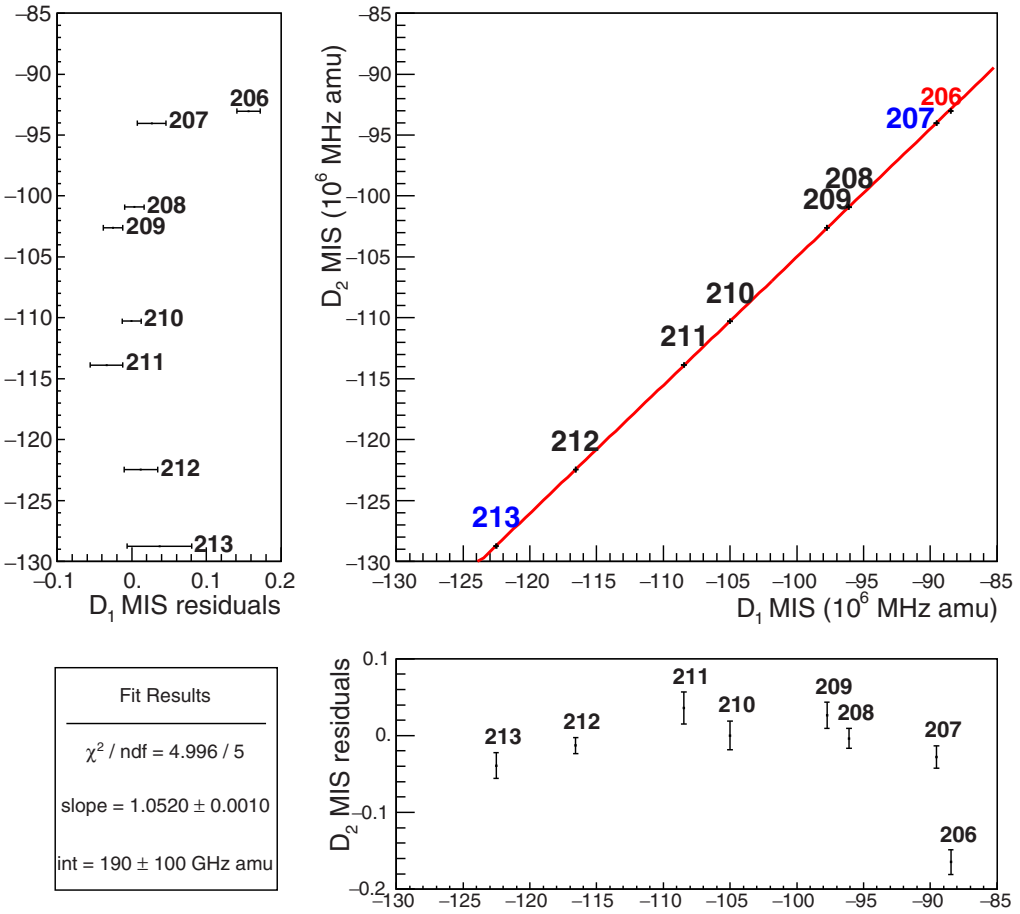

FIG. 4. (Color online) King plot of the modified isotope shifts (MIS) on the D_2 and D_1 lines for francium. Existing D_2 line isotope shifts are recalculated using ^{221}Fr as the reference isotope. We provide results for $^{206-213}$Fr D_1 isotope shifts. The slope of the fitted line gives the ratio of the field shift constants for the two transitions. The intercept provides the corresponding difference in the mass shift constants. Plots of the D_1 and D_2 residuals are shown. The blue ^{207,213}Fr are from the first experimental run data and the black $^{208-212}$Fr are from the second run data. The red ^{206}Fr point is not used in the fit for reasons explored in the text.

by typically a factor of two due to the uncertainties of the ground-state A coefficients alone. Improving the experimental result would require more precisely measuring both of these quantities.

V. SUMMARY

We have measured isotope shifts on the D_1 line in $^{206-213}$Fr with respect to ^{221}Fr using a fast rf sweep of laser sidebands. A King plot allows us to separate the field shifts ratio, $F_{D2}/F_{D1} = 1.0520(10)$, and mass shifts in these isotopes and we deduced the specific mass shifts relation, $S_{D2} - S_{D1}\frac{F_{D2}}{F_{D1}} = 170(100)$ GHz amu, in good agreement with the theory predictions.

ACKNOWLEDGMENTS

The authors would like to thank the ISAC staff at TRIUMF for developing the Fr beam. This work is supported by NRC, TRIUMF, and NSERC from Canada, U.S. Department of Energy and U.S. NSF, and CONACYT from Mexico. R.C. acknowledges financial support from a University of Manitoba Graduate Fellowship.

[1] W. Nörtershäuser, R. Sánchez, G. Ewald, A. Dax, J. Behr, P. Bricault, B. A. Bushaw, J. Dilling, M. Dombsky, G. W. F. Drake, S. Götte, H.-J. Kluge, T. Kühl, J. Lassen, C. D. P. Levy, K. Pachucki, M. Pearson, M. Puchalski, A. Wojtaszek, Z.-C. Yan, and C. Zimmermann, Phys. Rev. A **83**, 012516 (2011).

[2] A. Nieminen, P. Campbell, J. Billowes, D. H. Forest, J. A. R. Griffith, J. Huikari, A. Jokinen, I. D. Moore, R. Moore, G. Tungate, and J. Äystö, Phys. Rev. Lett. **88**, 094801 (2002).

[3] M. G. Kozlov, V. A. Korol, J. C. Berengut, V. A. Dzuba, and V. V. Flambaum, Phys. Rev. A **70**, 062108 (2004).

[4] W. Aoki, S. G. Ryan, J. E. Norris, T. C. Beers, H. Ando, N. Iwamoto, T. Kajino, G. J. Mathews, and M. Y. Fujimoto, Astrophys. J. **561**, 346 (2001).

[5] J. Ginges and V. Flambaum, Phys. Rep. **397**, 63 (2004).

[6] M. J. Ramsey-Musolf and S. A. Page, Ann. Rev. Nucl. Part. Sci. **56**, 1 (2006).

[7] G. Gwinner, E. Gomez, L. Orozco, A. Perez Galvan, D. Sheng, Y. Zhao, G. Sprouse, J. Behr, K. Jackson, M. Pearson, S. Aubin, and V. Flambaum, Hyperfine Interact. **172**, 45 (2006).
[8] V. A. Dzuba, W. R. Johnson, and M. S. Safronova, Phys. Rev. A **72**, 022503 (2005).
[9] K. Heilig and A. Steudel, At. Data Nucl. Data Tables **14**, 613 (1974).
[10] W. H. King, *Isotope Shifts in Atomic Spectra*, Physics of Atoms and Molecules (Plenum, New York, 1984).
[11] M. Tandecki, J. Zhang, R. Collister, S. Aubin, J. A. Behr, E. Gomez, G. Gwinner, L. A. Orozco, and M. R. Pearson, J. Instrum. **8**, P12006 (2013).
[12] J. Zhang *et al.* (unpublished).
[13] W. Z. Zhao, J. E. Simsarian, L. A. Orozco, and G. D. Sprouse, Rev. Sci. Instrum. **69**, 3737 (1998).
[14] See, e.g., C. J. Foot, Contemp. Phys. **32**, 369 (1991).
[15] J. E. Simsarian, L. A. Orozco, G. D. Sprouse, and W. Z. Zhao, Phys. Rev. A **57**, 2448 (1998).
[16] A. Coc, C. Thibault, F. Touchard, H. Duong, P. Juncar, S. Liberman, J. Pinard, J. Lermé, J. Vialle, S. Büttgenbach, A. Mueller, and A. Pesnelle, Phys. Lett. B **163**, 66 (1985).
[17] A. Voss, M. R. Pearson, J. Billowes, F. Buchinger, B. Cheal, J. E. Crawford, A. A. Kwiatkowski, C. D. Philip Levy, and O. Shelbaya, Phys. Rev. Lett. **111**, 122501 (2013).
[18] S. Sanguinetti, R. Calabrese, L. Corradi, A. Dainelli, A. Khanbekyan, E. Mariotti, C. de Mauro, P. Minguzzi, L. Moi, G. Stancari, L. Tomassetti, and S. Veronesi, Opt. Lett. **34**, 893 (2009).
[19] H. T. Duong, P. Juncar, S. Liberman, A. C. Mueller, R. Neugart, E. W. Otten, B. Peuse, J. Pinard, H. H. Stroke, C. Thibault, F. Touchard, J. L. Vialle, K. Wendt (ISOLDE Collaboration), Europhys. Lett. **3**, 175 (1987).
[20] G. Audi, O. Bersillon, J. Blachot, and A. Wapstra, Nucl. Phys. A **729**, 3 (2003).
[21] S. A. Blundell, P. E. G. Baird, C. W. P. Palmer, D. N. Stacey, and G. K. Woodgate, J. Phys. B **20**, 3663 (1987).
[22] I. Angeli, Acta Phys. Hungarica A **17**, 3 (2003).
[23] A.-M. Mårtensson-Pendrill, Mol. Phys. **98**, 1201 (2000).